Investigate the Wake Flow on Houseflies with Particle-Tracking-Velocimetry and Schlieren Photography

Yun Liu*, Angel David Lozano

Department of Mechanical and Civil Engineering, Purdue University Northwest, Westville, IN 46323, USA.

Abstract

Utilizing high-speed schlieren photography and particle-image-velocimetry, the wake flow of tethered houseflies is investigated. The high-speed schlieren photography is implemented on tethered houseflies inside an air container with a stable vertical temperature gradient to visualize the disturbed wake flow from the insects. The resulting photography images were then processed with the physics based optical flow method to derive the light-path averaged flow velocity. Additionally, the state of the art: Shake-the-Box system is implemented on a tethered housefly to measure the volumetric flow field in the wake of the insect, revealing interesting flow behavior and structures that can also be observed and correlated to the schlieren photography experiment results. Comparing the dimensionless velocity magnitude of the wake flow from the two experiments, a good qualitative agreement is reached, suggesting the viability of high-speed schlieren photography in investigating the wake flow of small insects. Furthermore, the high-speed schlieren photography is successfully applied on a housefly that is taking off from the ground, visualizing the disturbed wake flow on the freely flying insect that is challenging to achieve with other methods.

Keywords: Insect flight, Schlieren photography, Shake-The-Box, Wake flow

1. Introduction

Insects flap their flexible membrane wings in the air, creating complex wake flow that is highly unsteady and three-dimensional. In return, transient aerodynamic forces are produced on the flapping wings, realizing extraordinary flying and maneuvering abilities [1]. To investigate the associated aerodynamics and flow physics of insect flight, enormous flow visualizations and measurements have been carried out on a wide range of insect species. Qualitative smoke/smoke wire visualizations were extensively implemented on tethered or freely flying insects to observe the flow patterns and structures formed around the insect wings. On tethered Hawkmoth *Manduca sexta*, a cone shaped Leading Edge Vortex (LEV) was captured and visualized with smoke wire visualization, leading to an important discovery of lift augmenting mechanics on insect wings [2]. On freely flying butterflies, smoke wire visualization revealed different flow phenomena and distinct flow structures at different stages of flapping wing cycle, suggesting the insects might implement different unsteady aerodynamic mechanisms during the flight [3]. On freely flying bubble bees, independent leading-edge vortices and vortical flow structures were visualized on each wing through smoke wire visualization [4]. On flying beetle, the smoke wire visualization was implemented under different flying conditions, including hovering, forward and climbing flights, capturing the behaviors of different flow structures, and revealing the functions of the elytron (the hardened forewings of beetles) in vortical flow formation [5]. On the other hand, to quantitatively investigate the flow field on flapping wings, two-dimensional Digital Particle Image Velocimetry has been widely implemented [6-8]. On tethered Tobacco Hawkmoths, two-dimensional Digital Particle Image Velocimetry (2D-PIV) was implemented in a low-speed wind tunnel. At the end of the down-stroke, a significant leading-edge vortex flow feature is

* Author to whom correspondence should be addressed: liu739@pnw.edu

captured while the aerodynamic force is measured on the tethered insects [8]. The Digital Particle Image Velocimetry (DPIV) was also implemented on freely flying hawkmoths, revealing a dynamic and complicated leading-edge vortex structure consists of multiple vortex cores [9]. Moreover, the DPIV was carried out on other tethered insects, such as locust, fruit fly and mosquito, revealing quantitative 2-dimensional flow field of their flapping wings [10-12].

With those early implementations of conventional flow visualization and measurement techniques, although some flow details and aerodynamic physics have been discovered and revealed, the majority of these conventional flow studies are limited to either qualitative flow visualization on incomplete flow structures or quantitative flow field measurements on two-dimensional planes; whereas, the actual flow structures on flying insects are complicated in the three-dimensional space. Recent advancement in three-dimensional particle tracking and flow reconstruction has enabled the volumetric flow measurement in all the three-dimensions and has been continuously improving. Defocusing-DPIV was utilized to study the three-dimensional flow field on translating and rotating plates in a water tank. The differences between the three-dimensional flow structures of translating and rotating wings were captured and studied in an unprecedented detail [13]. In an oil tank, the Defocusing-DPIV method was implemented on mechanical flappers with transparent wings, revealing strong three-dimensional effects of the flow which is continuously deforming and convecting [14, 15]. Tomographic PIV, on the other hand, is extensively implemented in studying the complex three-dimensional flow phenomena of insect flight in the air. A large volume Tomographic PIV measurement was carried out in the wake of a tethered locust with a low-speed wind tunnel [16]. Details on instantaneous three-dimensional vortical flow field and its development were quantitatively visualized and investigated with some interesting flow phenomenon observed, including the wake deformation, secondary vortical flow structures and shear layers. The Tomographic PIV experiment was also implemented on a freely hovering hummingbird hawkmoth in the wake below the insect, capturing series of bilateral, stacked vortex rings [17]. However, in both studies, only in the far-field wake region away from the wings, the three-dimensional flow measurement and visualization were enabled, leaving the three-dimensional unsteady flow field information close to the wings still unclear.

To visualize the entire three-dimensional flow structures on flying insects, the high-speed schlieren photography was recently introduced and implemented on freely flying hawkmoths [18]. In the beginning, isopropyl alcohol was brushed on the surfaces of hawkmoth wings and then the insect was released to fly in a schlieren photography system with two high-speed cameras filming from two different perspectives. The alcohol vapor, shed from the insect wings, behaves like passive scalar that tracks the vortex structure formation shed from the insect wings. The images of vortex structures were successfully visualized and captured from the high-speed schlieren photography on the freely flying hawkmoths. Moreover, the filaments of vortex structures were three-dimensionally reconstructed from the schlieren images using direct linear transformation and compared to a numerical simulation study [19]. However, the method is not applicable to small insects like housefly or fruit fly that cannot bear the weight of the isopropyl alcohol on their wings. In this study, a new method is introduced on houseflies to visualize the wake flow formation with schlieren photography. Moreover, the physics-based optical flow method [20, 21] is applied to the schlieren photography images to quantify the light-path averaged flow velocity. In a recent study on flying owls, an advanced Particle Tracking Velocimetry (PTV) system of the Shake-The-Box was implemented to investigate the wake flow field of down-wash, revealing advanced volumetric flow measurement capability of the system [22]. Particularly, the Shake-the-Box can significantly expedite the data processing to derive the three-dimensional flow field [23]. In this study, the Shake-the-Box system is implemented on tethered housefly to measure the volumetric flow field around houseflies for a quantitative comparison with the schlieren photography result.

2. Materials and Methods

Housefly pupae were obtained through an online vendor: Josh's Frogs Ltd. Once pupae hatched, the insects were tethered utilizing a UV light repair glue to a pole for the tethered flight experiments. The high-speed schlieren photography has been successfully implemented on flying hawkmoths with alcohol vapor brushed the wing surfaces [18]. However, on small insects, this approach doesn't work since the small insects cannot bear the weight of alcohol. Therefore, in this study, a different method is introduced from implementing a vertical temperature gradient. Veldhuis studied the wake flow of rising bubbles in a water tank using schlieren photography [24]. A vertical temperature/density gradient was established from using a lamp above the tank to heat the water from the top. When the air bubbles raised into the temperature/density gradient field, the wake disturbed the density gradient field, and the disturbance was then captured and visualized through the schlieren imaging. Inspired by Veldhuis' work, we built a vertical temperature gradient inside an air container (76 × 40 × 50 mm) on which an electric heating plate was placed at the top and a cold-water cooling plate installed at the bottom with temperature-controlled power modules to regulate the temperatures. When the system reaches the equilibrium state, the top of container stays at a temperature of 62 ºC and the bottom stays at a temperature of 14 ºC. The air container with temperature gradient is placed in a parallel light schlieren photography system with the optical glasses facing the parallel light of the system. The schlieren photography system has two 10-inch parabolic mirrors (Edmund Optics) to collimate the light originated from the LED through a 1mm pin hole. As the light enters the container perpendicular to the optical glasses, the light is not refracted, therefore eliminating the image distortion due to the container walls. At the focal point of the light, a razor blade is vertically placed to create the schlieren imaging. Consequently, the schlieren images of disturbed flow field are taken by a high-speed camera (Mini UX 100, Photron) at a frame rate of 10000 fps.

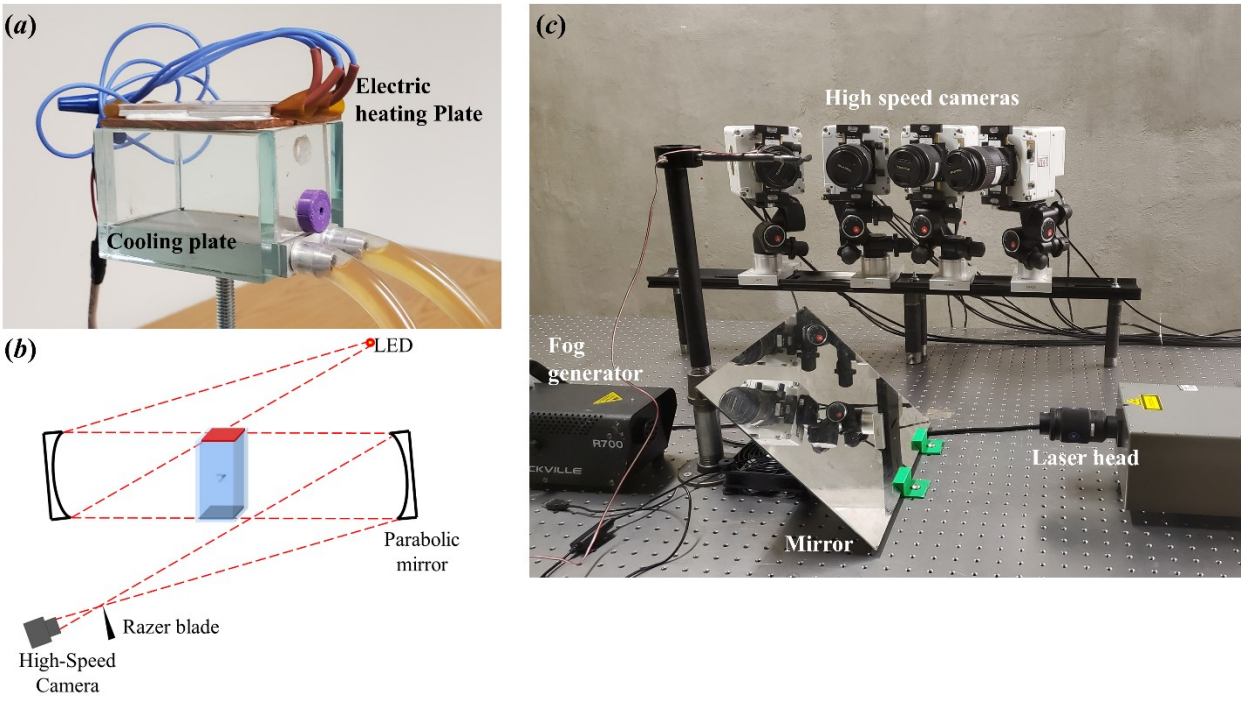

Figure 1. *a*) Air container with a vertical temperature gradient, built with electric heating plate on the top and cold water cooling plate at the bottom. *b*) Parallel light schlieren photography setup to visualize disturbed wake flow structures. *c*) Experimental setup for the volumetric flow measurement (Shake-the-Box)

To derive quantitative flow field data from the schlieren photography images, the physics based optical flow method is implemented on the collected schlieren images on tethered houseflies. Based on the traditional optical flow method, Liu and Shen developed a physics-based optical flow method which is

capable of analyzing schlieren images with continuous distribution of brightness and density [20]. From considering the actual behavior of the viscous fluid, Liu and Shen modified the conventional brightness constrain equation ($\frac{\partial g}{\partial t} + \nabla \cdot (g\boldsymbol{u}) = 0$) by introducing fluid diffusion and boundary effects. From solving the new equation ($\frac{\partial g}{\partial t} + \nabla \cdot (g\boldsymbol{u}) = f(x_1, x_2, g)$), a new optical flow vector field, which represents the actual fluid flow, can be derived. However, as the schlieren images represent the integral result of the light refraction over the volumetric field of interest, the optical flow method quantifies only the path-averaged velocity over the traveling path of the light.

The state-of-the-art: Shake-the-Box system (Lavision, Gottingen) is implemented on tethered houseflies to measure the volumetric velocity field in the wake of the flapping wings. The laboratory space is seeded with 1~5 microns fog particles (R700 Rockville Fog generator). A high repetition rate Nd: YLF single cavity laser (Photonics DM-30-527, 30 mJ/pulse at 1 kHz with a wavelength of 527 nm) and four high-speed cameras (Phantom VEO 640), on the same side, were utilized to illuminate the particles in the flow field and to film the particle images. The lenses (Tokina Macro) have a focal length of 100 mms and are set at aperture size of f-4.5 during the experiments. Cylindrical optical lens is added on the laser head to generate an 8 mm thick laser light volume below the insect in the wake. And an inclined mirror is utilized to redirect the laser light vertically so that the wake below the insect wings can be fully illuminated. To measure and resolve the unsteady flow field within a volume of 30×30×5 mm, the sampling frequency of the images was set at 4.5 kHz (repetition rate of the laser and cameras) with an image resolution of 1024×1024 pixels on all the four high-speed cameras. The calibration, data collection and velocity field constructions were realized using the software Davis 10 (LaVision, Gottingen). A 55×55 mm calibrate target was utilized and placed in the field of view for taking the images by the high-speed cameras. Then the calibration was performed from the four images of the target in the Davis 10. Finally, the experiments were conducted on tethered houseflies with their wings flapping during the experiments. To realize the volumetric measurement with the system and improve sub-pixel accuracy, the volume self-calibration is required by the Shake-the-Box system. Therefore, volumetric self-calibration is carried out with the particle images taken during the experiments. Afterward, the particle reconstruction/tracking was carried out with the Shake-the-Box algorithm (LaVision, Gottingen) through shaking the particle position by 1 voxels during the iterations and the instantaneous volumetric velocity field was eventually reconstructed through the post-processing within the Davis 10, resulting three 40×40×8 matrices for the volumetric velocity in the three dimensions with a spatial resolution of 0.762 mm/velocity vector. For details about the algorithm of Shake-The-Box, please refer to Schanz et al [23].

3. Results and Discussion

3.1 Flow structure and velocity field from schlieren photography

Figure 2 shows a sequence of schlieren photography images on a tethered housefly with a Tip-Root Wing length of 5.6 mm, focusing on the near wake flow close to the insect. During the down-stroke, a horseshoe vortex structure is created on each wing of the housefly with clear images of tip and root vortices. The horseshoe vortex structures shed at the end of the down-stroke and evolves into a vortex loop. Then, during the upstroke, tip and root vortices are generated again and linked to the shed vortex loop from the down-stroke, consequently, forming a linked vortical wake structure after one wing beat cycle (The supplementary video SV1 shows the sequence of the vortex structures and their evolutions).

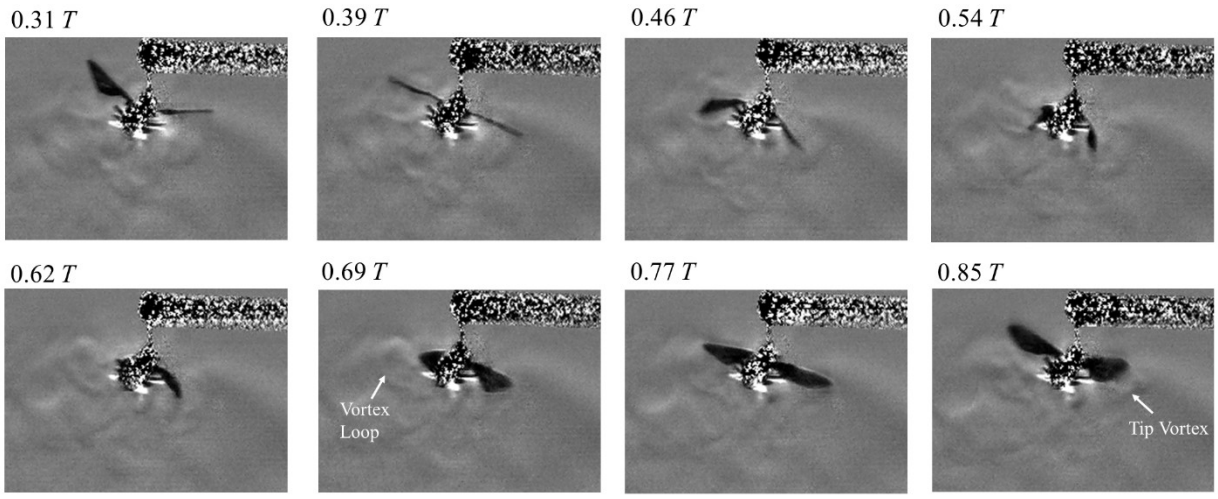

Figure 2. A sequence of schlieren photography images on a tethered housefly with near wing vortex structure were captured and visualized. (Supplementary video SM1 is provided)

Figure 3 presents a sequence of schlieren images on the tethered housefly, focusing on the entire wake flow, including the near- and far- wake flow. Meanwhile, the optical flow method derived velocity vector field within a 437×323 pixels domain is presented below the corresponding schlieren images (Since the wing motion interferes with the optical flow algorithm and introduces pseudo flow velocities, the flow field away from the insect is analyzed and presented). As the insect is slightly titled from the horizontal plane, the created wake flow is not perfectly vertical and slightly titled. Over the complete wing beat cycle, the wake flow field is primarily dominated by the downward momentum imposed from the flapping wings. Noticeably, the downward momentum is more significant during the down-stroke (A larger region of high downward moment observed at 0.32T and 0.48 T) but weaker during the upstroke (A smaller region of downward moment observed at 0.32T and 0.48 T). This observation can be further verified from calculating the averaged downward velocity in a fixed rectangular domain of 26×210 pixels (0.52 × 4.2 wing length) below the insect. Figure 4 presents the mean downward velocity considered in the domain. The mean downward velocity in the considered region reaches the maximum value of 0.55 m/s at 0.44 T and stays slightly higher during the down-stroke from 0.2 T to 0.5 T while the downward velocity is slightly lower during the upstroke.

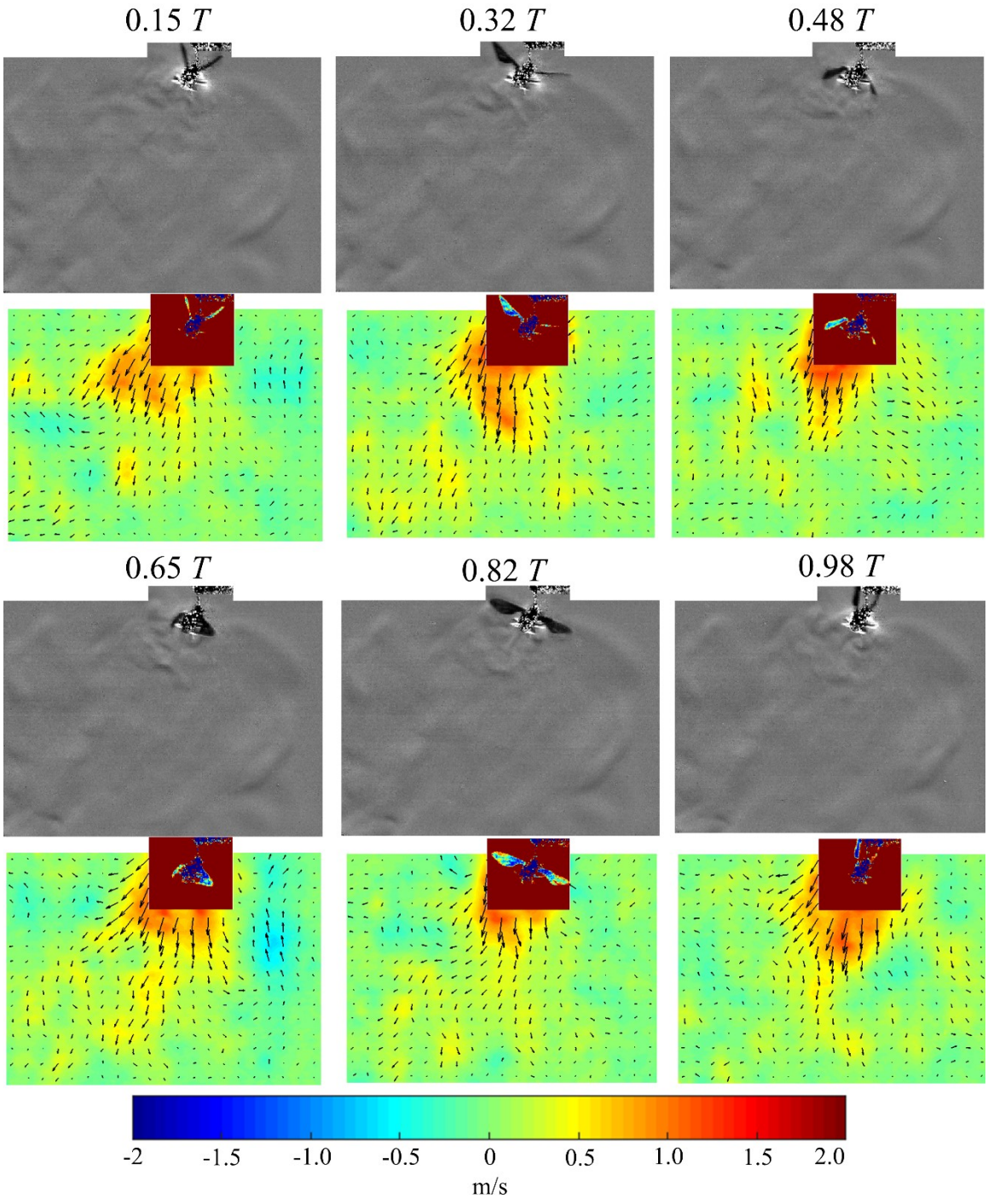

Figure 3. A sequence of schlieren photography images on a tethered housefly and their corresponding light-path averaged velocity field derived using the physics-based optical flow method.

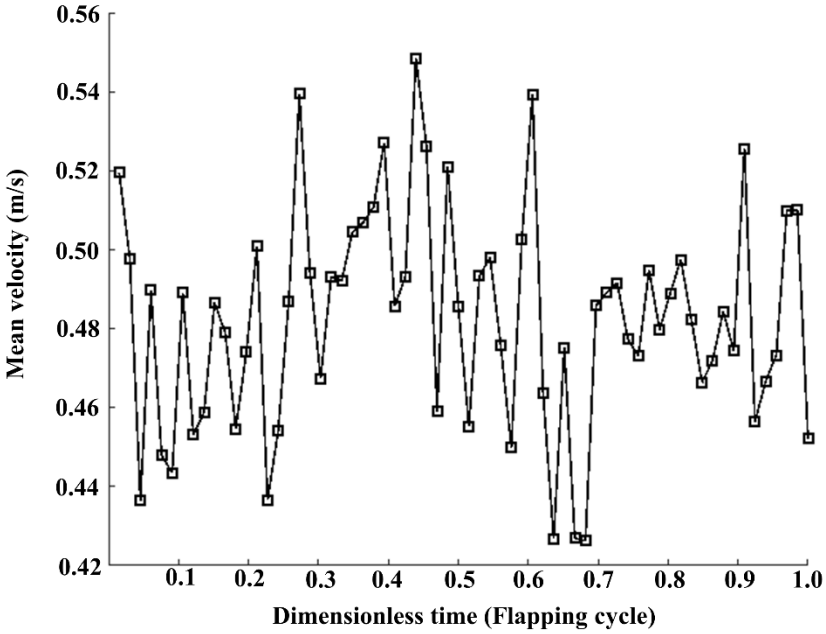

Figure 4. Mean downwash velocity estimated within a domain of the 0.52 wing-length × 4.2 wing-length at 1.0 wing-length below the insect.

3.2 Vorticity field from volumetric flow measurement.

Figures 5, 6 and 7 present the ensemble/cycle averaged results of volumetric flow field derived from the Shake-the-Box system on a tethered housefly with a wing length of 5.8 mm over one wing beat cycle. As the volumetric flow can only be acquired in the region away from the insect wings, therefore, the presented flow field results should be considered as far-wake flow field that is not on the insect wings. Figure 5 shows the velocity vector field and the iso-surface of the vorticity in the x direction (normal to the sagittal plane of the insect body). The red surface enclosed the region where the vorticity ω_x is equal to or larger than 250/s while the blue surface enclosed the region where the vorticity ω_x is equal to or lower than -250/s. To our surprise, the distribution of x direction vorticity is highly disproportional. And the majority part of the flow field is dominated by the flow rotation in the positive x direction, indicated by the red surface domain, while the flow rotation in the opposite direction is distributed in limited regions, in the blue surface confined region. Moreover, this observation is evident over the entire wing flapping cycle, suggesting the vorticity field normal to the sagittal plane is always dominated by positive vorticity in the x direction which is the same direction as the leading edge vortex flow on insect wings. Nevertheless, the vorticity generation in y direction (vertical axis) is much more proportional and well balanced. Figure 6 presents the iso-surface of the vorticity in y direction. The red surface enclosed the region where the vorticity ω_y is equal or larger than 250/s while the blue surface enclosed the region where the vorticity ω_y is equal or lower than -250/s. Elongated structures are observed in the beginning of the down-stroke and the end of the upstroke, which can be correlated to the formation of the tip and root vortices during the upstroke as the fluid rotates in the vertical direction. Figure 7 presents the iso-surface of the vorticity in the z direction. The red surface enclosed the region where the vorticity ω_z is equal or larger than 250/s while the blue surface enclosed the region where the vorticity ω_z is equal or lower than -250/s. As expected, two major shearing flow structures are created between the downwash flow and the ambient air which can be visualized and captured by the vorticity in the z direction.

To have a better understanding on the distribution of vorticity, the vorticity are replotted on the frontal plane (Coronal plane). Figures 8, 9 and 10 present the instantaneous streamline pattern and instantaneous pseudo color plots of vorticity ω_x, ω_y and ω_z on the frontal plane. The streamline patterns depict the downwash wake flow region with clear boundaries that clearly separates the downwash wake flow and the ambient air

while the vortical flow is predominately distributed within the boundaries. In the X direction, the positive vorticity of ω_x dominates the entire wake flow field over the entire wing beat cycle, which further supports our previous observation on the disproportional distribution of ω_x. In the wake away from the insect, at the beginning of down-stroke (t = 0 T), negative ω_x first appeared in the flow field then it convects downward with its strength weakening over time during the rest of time. However, at t = 0.19 T, positive ω_x moved into the downwash flow field and is rapidly strengthening over the wing beat cycle. In the next wing beat, the positive ω_x starts weakening as it moves away from the wing. Therefore, several wing-beat cycles after wing start flapping, a wake flow field with predominantly positive X vorticity is established in the wake. Similar to the observation in Figure 6, the distribution of ω_y in Figure 9 is more proportionally distributed on the frontal plane. Moreover, the vorticity ω_y is found to be strengthening only during the up-stroke which is consistent with the observation in the Figure 6, correlating the vertical direction vorticity ω_y to the tip and root vortices that are mainly formed during the up-stroke. In Figure 10, during the down-stroke, two significant vortex pairs in z direction are created and convect with the downwash flow over time while no new ω_z is created on frontal plane during the upstroke. Furthermore, to study the proportion of the vorticity distribution in each direction, the magnitude of the sum of the positive and negative vorticity in each direction are calculated within the measurement domain and plotted in Figure 11 *a*. While the total negative and positive vorticity are well balanced in the Y and Z direction, in X direction, the magnitude of the total positive vorticity is significantly higher than the magnitude of the total negative vorticity which supporting our earlier observation in Figures 5-10. Consequently, the volumetric flow measurement results imply that the vorticity in the horizontal directions (ω_x and ω_z) are primarily created during the down-stroke while the vorticity in vertical direction (ω_y) is primarily generated during the up-stroke. In addition, the negative and positive vorticity in the Y and Z direction (ω_y and ω_z) are distributed proportionally while the positive vorticity magnitude in X direction is more significant than its negative vorticity.

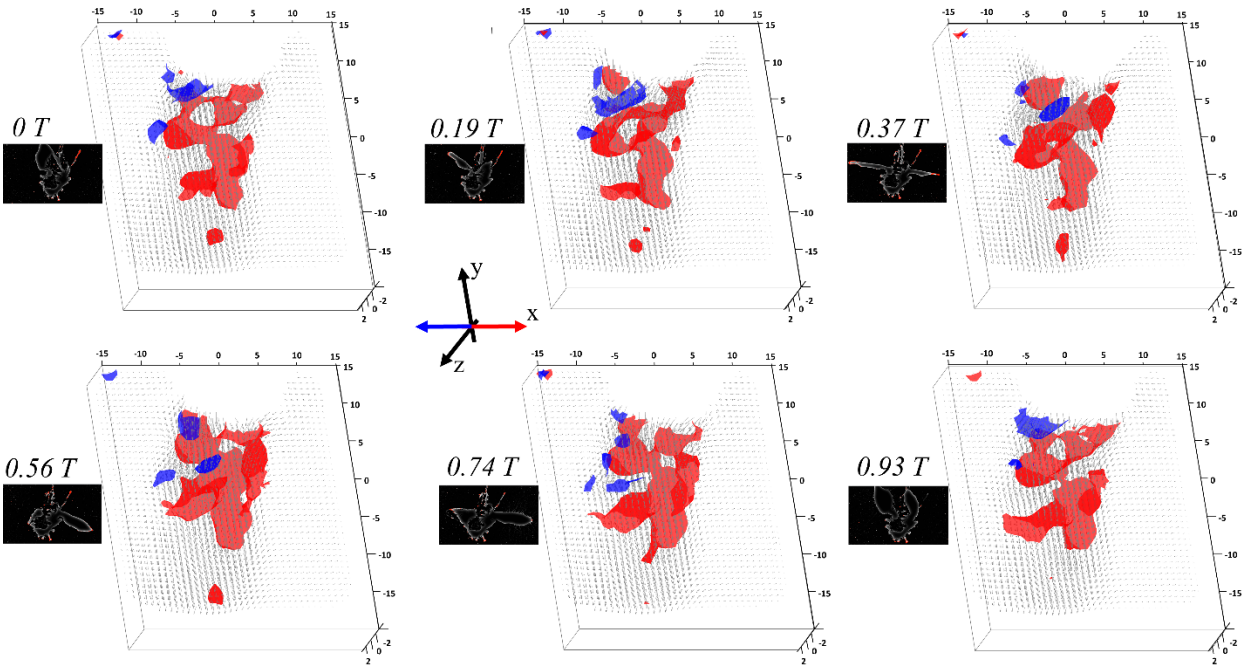

Figure 5. Volumetric flow measurement result on a tethered housefly. Red surface represents iso-surface of ω_x = 250/s; Blue surface represents iso-surface of ω_x = - 250/s;

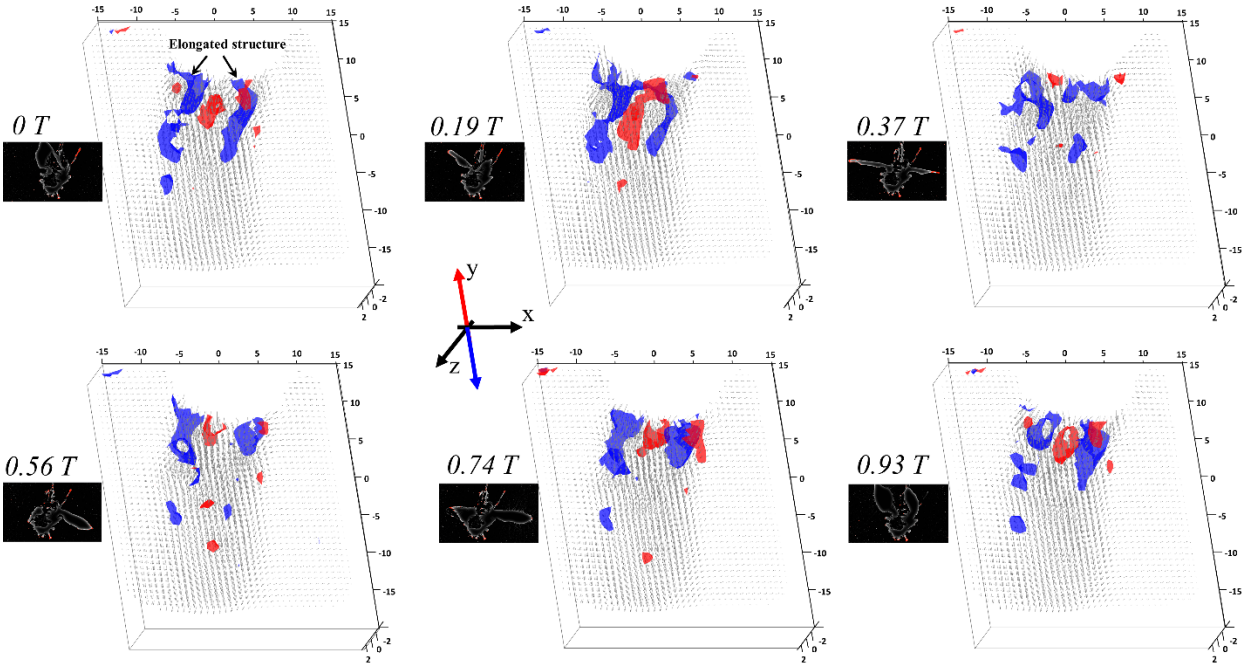

Figure 6. Red surface represents iso-surface of ω_y = 250/s; Blue surface represents iso-surface of ω_y = -250/s;

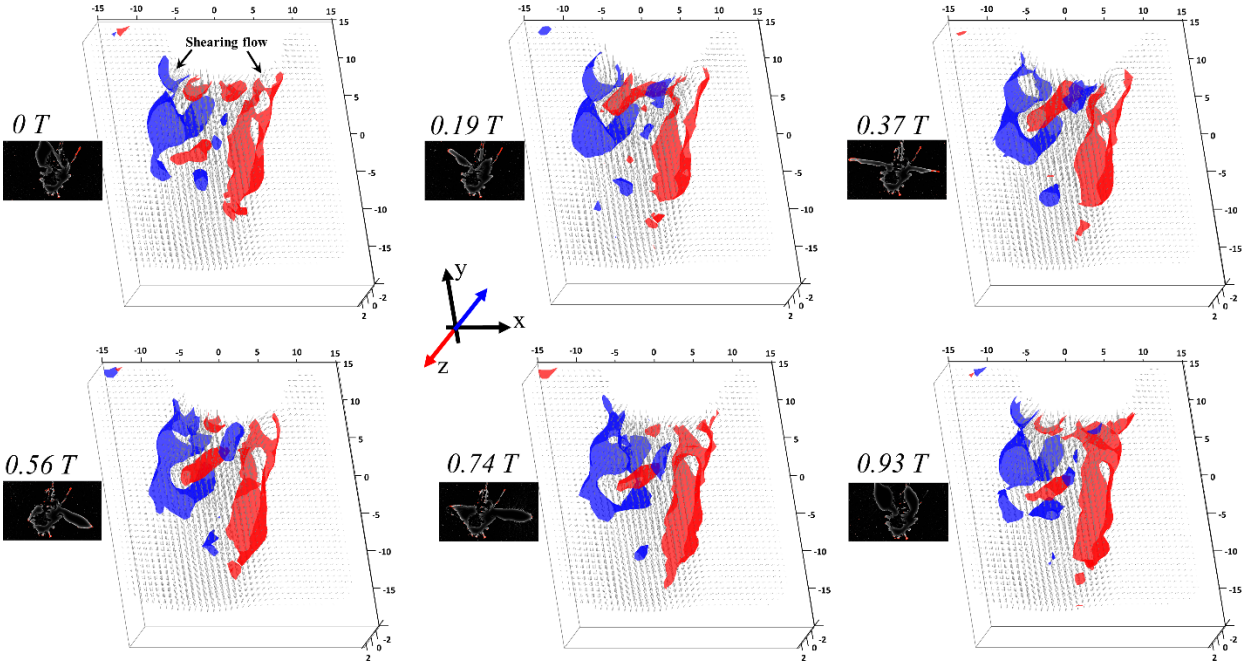

Figure 7. Red surface represents iso-surface of ω_z = 250/s; Blue surface represents iso-surface of ω_z = -250/s;

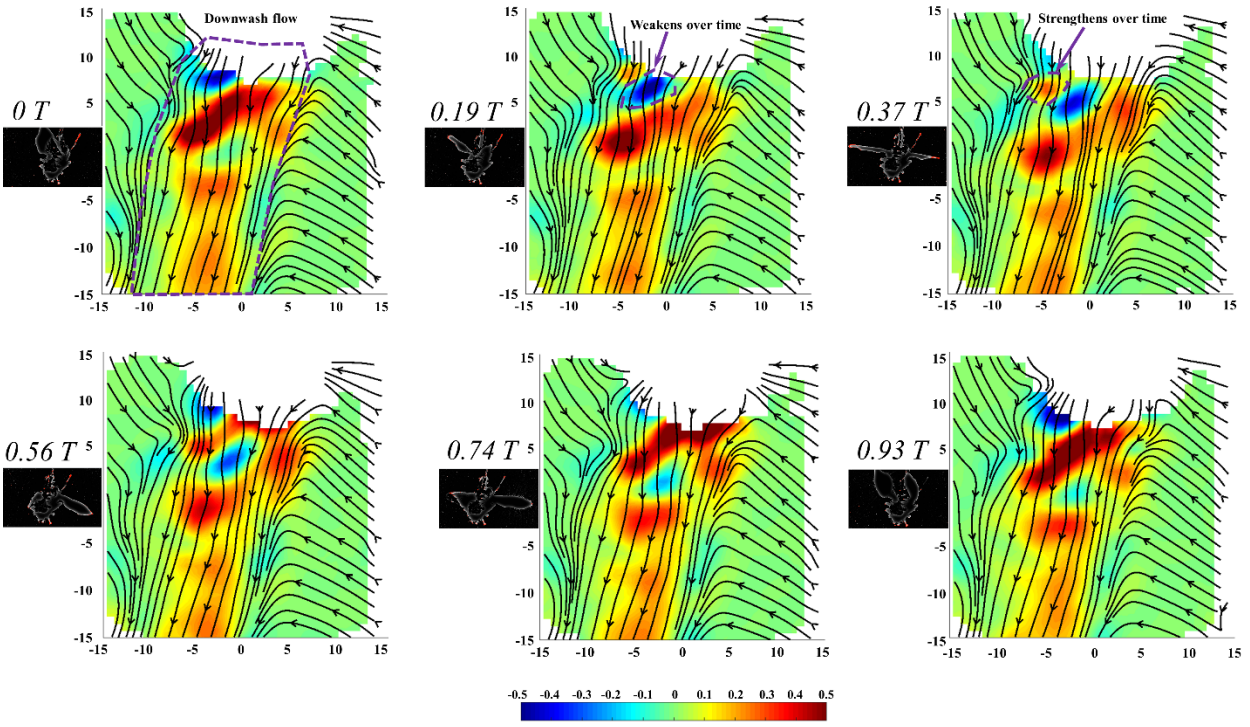

Figure 8. Volumetric flow measurement results on frontal plane. Pseudo color plot of vorticity ω_x and streamlines on frontal plane.

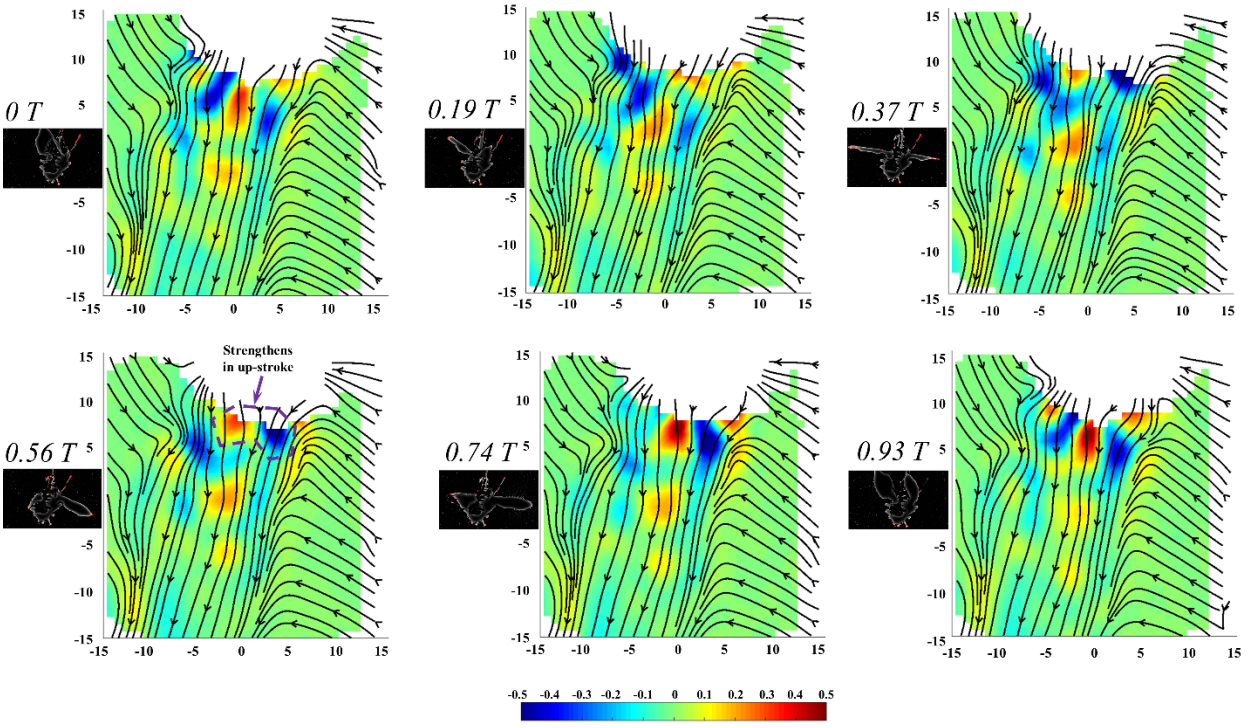

Figure 9. Pseudo color plot of vorticity ω_y and streamlines on frontal plane.

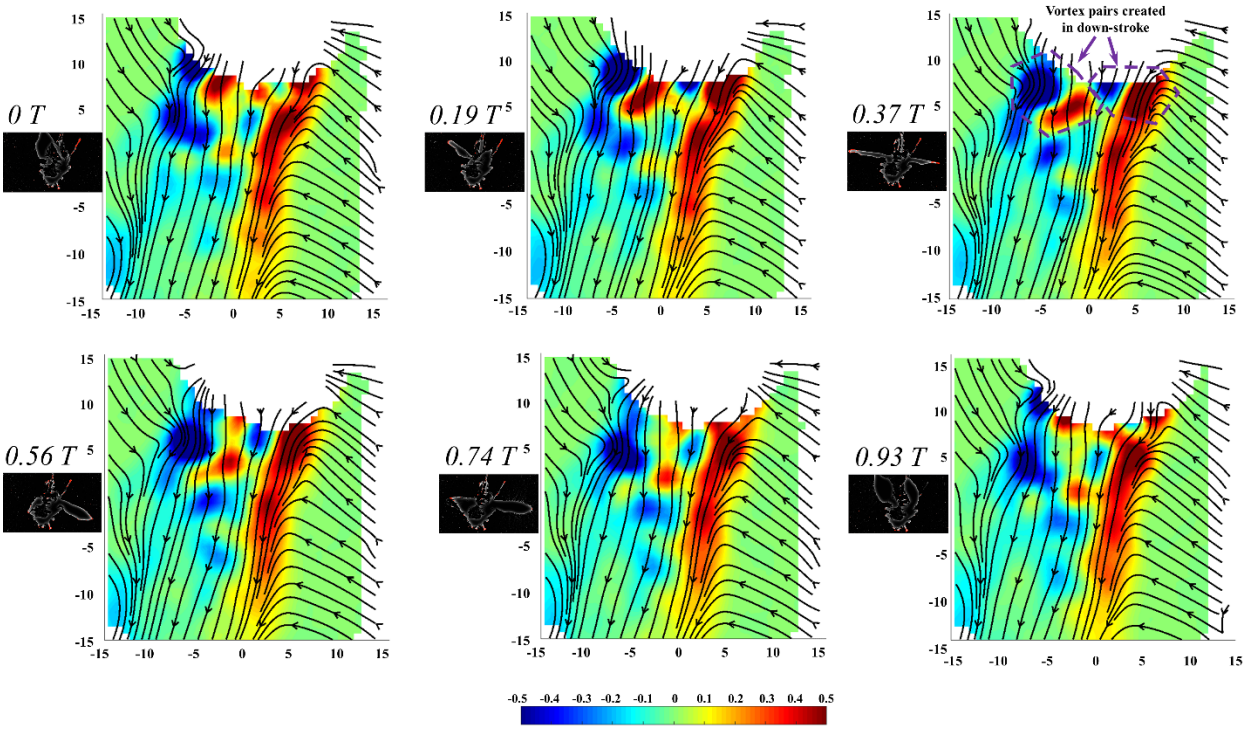

Figure 10. Pseudo color plot of vorticity ω_z and streamlines on frontal plane.

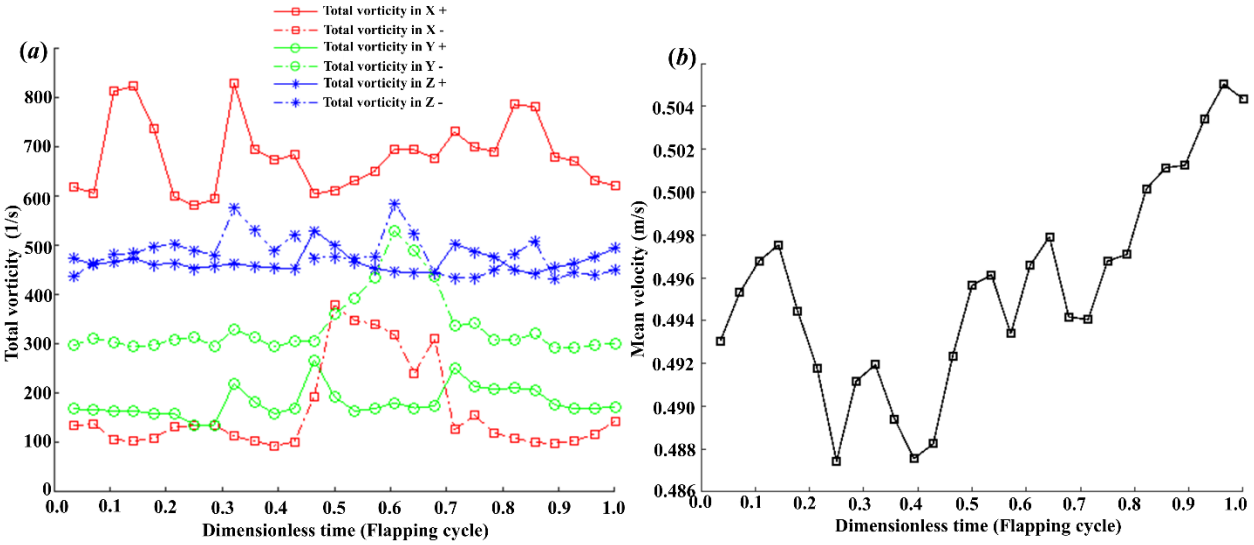

Figure 11. a) Sum of positive and negative vorticity over the measurement volume. b) Mean value of downwash velocity considered within a volume of 0.52 wing length × 4.2 wing length × measured volume thickness (5 mm) at 1.0 wing length below the tethered insect.

Meanwhile, similar to the analysis of schlieren photography result, the mean downwash velocity is considered and estimated at 5.8 mm (1.0 wing length) below the tail of the tethered housefly within a volume of 3.0 mm × 24.4 mm × 5.4 mm (0.52 wing length × 4.2 wing length × the thickness of the flow resolved flow field) and the result is presented in Figure 11 b. Over one wing beat cycle, the mean downwash velocity varies slightly in the range between 0.488 and 0.505 m/s. However, contradicting to the schlieren photography result, the lower downwash velocity is observed at the down-stroke while the higher

velocity is seen during the up-stroke. Since the mean velocity is estimated within a 5.4 mm thick volume, the downwash flow might go outside the volume as convecting downward, leading to the discrepancy. As the particle tracking velocimetry experiment and schlieren photography experiment were conducted on different insects, the differences in velocity field are expected. Moreover, the downwash flow from both experiments are clearly tilted to one side. Therefore, to compare the mean velocity magnitude between the two experiments, the magnitude of dimensionless velocity should be calculated by adding the horizontal velocity component u_x (Velocity u_z is not considered because it does not affect schlieren photography result and the dimensionless velocity is calculated by dividing the wing length/time duration of one wing beat). Figure 12 presents the comparison of dimensionless velocity magnitude from the two experiments estimated within the rectangular region (0.52 wing length × 4.2 wing length). While the particle tracking velocimetry derived dimensionless velocity magnitude stays relative stable at around 0.6, the schlieren photography derived dimensionless velocity magnitude fluctuates significantly between 0.53 and 0.66. Despite of the difference in instantaneous value, a good agreement can be found in an averaged sense. The averaged value of dimensionless velocity magnitude is at 0.5965 for particle image velocimetry experiment and 0.5933 for schlieren photography experiment.

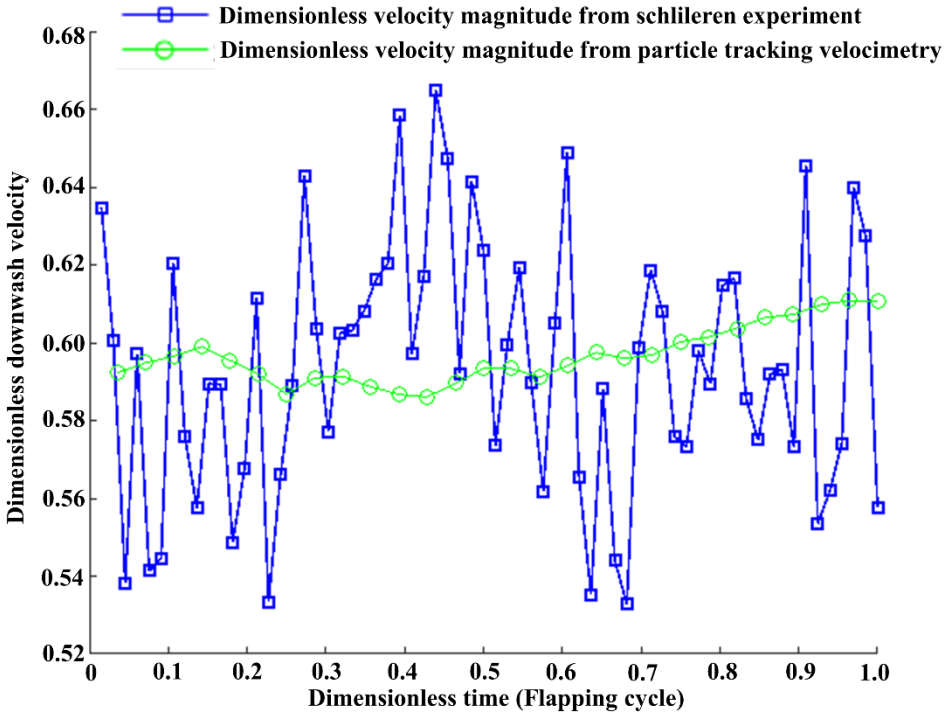

Figure 12. Comparison of dimensionless velocity magnitude between schlieren photography and particle image velocimetry.

3.3 Schlieren results on freely flying housefly.

Furthermore, the schlieren photography method was tried on houseflies without any restriction on their movement. In one trail, the flow pattern was captured on a housefly that was taking off from the bottom. The sequence of the schlieren photography images of one wing beat are presented in Figure 13 (The images are enhanced with background subtraction). Similar to the flow structures observed on the tethered insect, a bilateral structure is captured on the freely flying insect. During the down-stroke, a ring/pocket like structure is formed on each wing. Then during the up-stroke, the ring structure sheds and convects downward into the wake. However, unlike the schlieren photography images on the tethered insect, no clear tip vortex structure was captured on the freely flying insect during the up-stroke. While the Figure 13 only

presents the schlieren photography images over one wing beat cycle, the full video of the schlieren photography images is provided as the supplementary file SM 2.

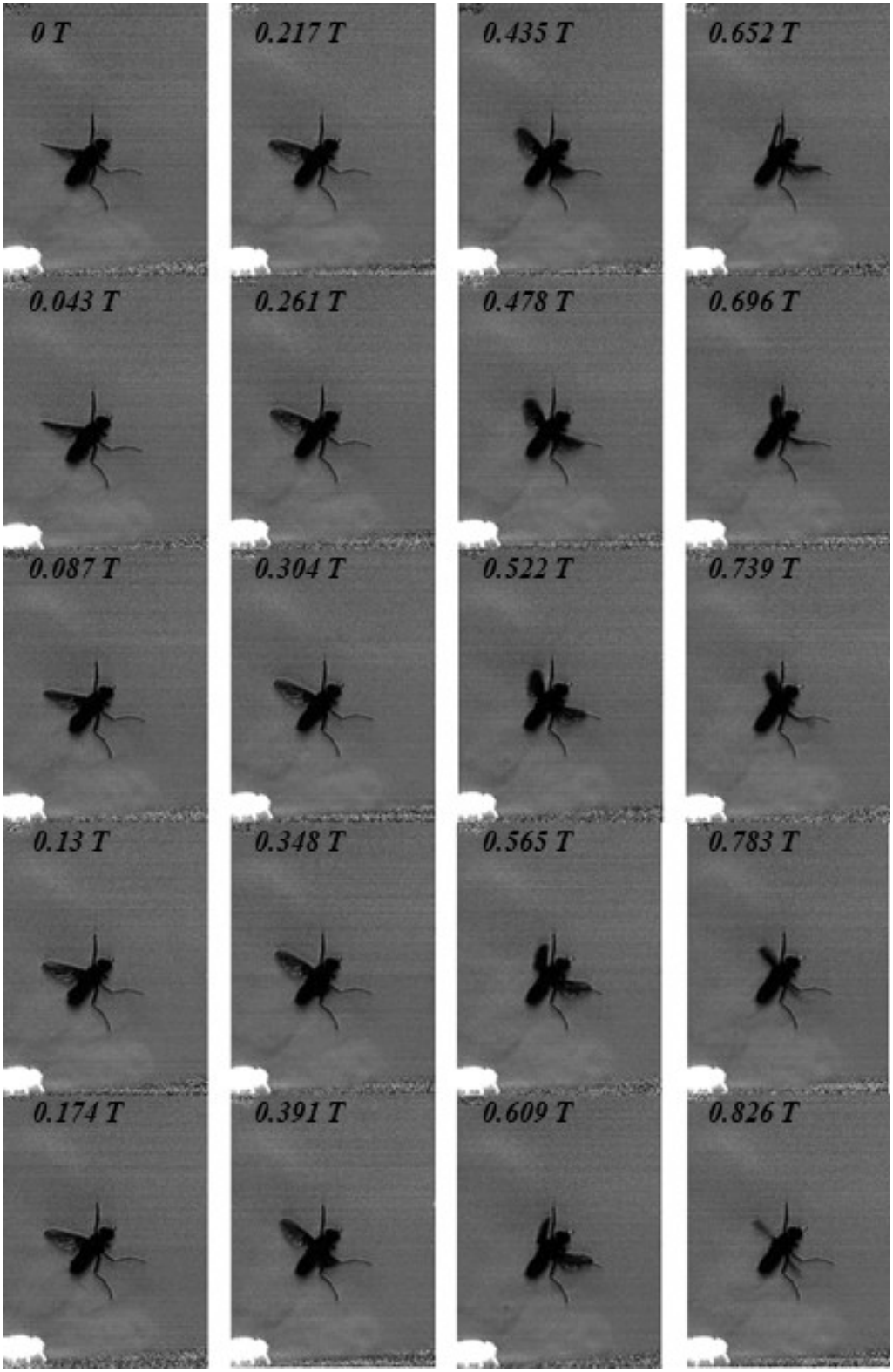

Figure 13. Schlieren photography on a freely flying housefly that is taking off from the ground.

4. Conclusion and Discussion

In this work, the high-speed schlieren photography and the Shake-The-Box system were utilized to study the wake flow of tethered houseflies. Different from the schlieren photography experiment on flying hawkmoths with alcohol vapor [18], a temperature gradient is established inside an optical glass container to visualize the disturbed wake flow of a tethered housefly. Similar to the schlieren photography study on freely flying hawkmoth, our schlieren photography study on the housefly reveals a similar bilateral vortex structure, consisting of a vortex loop created in the down-stroke and tip/root vortices formed in the up-stroke, on each wing. However, the secondary vortex structure that observed on hawkmoths' hind wings [18], was not captured on the housefly, suggesting the existence of hind-wing could be the main cause of secondary vortex structures. Meanwhile, the physics based optical flow method was applied on the schlieren photography images on the tethered housefly, deriving the light-path averaged velocity field. On the other hand, the particle-tracking-velocimetry experiment on the tethered housefly reveals detailed vortical flow behavior between the down- and up-stroke, showing the vorticity in horizontal directions (ω_x and ω_z) are primarily created during the down-stroke while vorticity in vertical direction (ω_y) is primarily formed during the up-stroke. For two-dimensional inviscid flow, according to the Kevin's circulation law, the magnitude of positive and negative in plane vorticity of a translating wing should be well balanced and the overall circulation of the flow field should be always zero if the total circulation starts at zero from the beginning [25]. Moreover, a numerical simulation on a translating wing suggests that even for viscous flow, at a Reynolds number of 1000, the overall circulation remains close to zero [26]. However, to our surprise, a significant disparity and disproportion of positive and negative vorticity distribution are observed in the direction normal to the sagittal plane (ω_x). A significant higher value of total vorticity (ω_x) is observed in the positive x direction than the value in the negative x direction while the values of total positive and negative vorticity are much more balanced in the z and y directions. From a numerical simulation on a flying hawkmoth [19], similar phenomena of disparity is observed in the direction normal to the sagittal plane, suggesting a possible generic wake flow behavior on flying insects. To further compare the wake flow velocity from the schlieren photography and particle tracking velocimetry experiments, the dimensionless velocity magnitude are calculated and compared in a similar flow domain, deriving a good agreement in velocity magnitude.

ACKNOWLEDGEMENTS

The Shake-The-Box system used for the particle tracking velocimetry experiment was funded by National Science Foundation (CMMI-1919726) to Y. Liu.

COMPETING INTEREST

The authors have no financial or non-financial interests in publishing this work.

DATA AVAILABILITY

The datasets generated during and/or analysed during the current study are available from the corresponding author on reasonable request.

References:

[1] Sane, S. P. (2003) The aerodynamics of insect flight. *Journal of Experimental Biology*. *206*, 4191-4208.

[2] Ellington, C. P., VandenBerg, C., Willmott, A. P., Thomas, A. L. R. (1996) Leading-edge vortices in insect flight. *Nature*, *384* 626-630,

[3] Srygley, R. B., Thomas. A. L. R. (2002)Unconventional lift-generating mechanisms in free-ying butteries. *Nature*, *206*(14) 660-664,

[4] Bomphrey, R. J., Taylor,G. K., Thomas, A. L.R. (2009) Smoke visualization of free-flying bumblebees indicates independent leading-edge vortices on each wing pair. *Experiments in Fluids*. *46*, 811-821,

[5] Truong, T., Le, T., Tran, H., Park, Yoon, H. K., Byun, D., (2012) Flow visualization of Rhinoceros Beetle in free flight. *Journal of Bionic Engineering*, *9,* 304-314,

[6] Altshuler, D., Princevac, M., Pan, H., Lozano, J. (2009) Wake patterns of the wings and tail of hovering hummingbirds. *Experiments in Fluids*, *46*, 835-846,

[7] Bomphrey, R. J., Lawson, N. J., Taylor,G. K., Thomas,A. L. R. (2006) Application of digital particle image velocimetry to insect aerodynamics: measurement of the leading-edge vortex and near wake of a Hawkmoth. *Experiments in Fluids*, *40* 546-554,

[8] Warrick,D. R., Tobalske, B. W., Powers, D. R. (2005) Aerodynamics of the hovering hummingbird. *Nature*, *435*, 1094-1097,

[9] Johansson, L. C., Engel, L. Kelbert, C., Heerenbrink, S. A., Hedenstrm, M.K. (2013) A.Multiple leading edge vortices of unexpected strength in freely ying hawkmoth, *Scientific Report*, *3,* 3264,

[10] Young, J., Walker, S., Bomphrey, R., Taylor, G. K., Thomas, A. L. R. (2009) Detials of instect wing design and deformation enchace aerodynamic function and flight efficiency, *Science*, 325, 1549-1552,

[11] Lehmann F., Wang, H., Engels, T. (2021) Vortex trapping recaptures energy in flying fruit flies, *Scientific Report*. *11* 6992,

[12] Bomphrey, R. J., Nakata, T., Phillips, N., Walker, S. M.(2017) Smart wing rotation and trailing-edge vortices enable high frequency mosquito flight, *Nature*, *544*, 92-95,

[13] Kim, D., Gharib, M. (2010) Experimental study of three-dimensional vortex structures in translating and rotating plates, *Experiments in Fluids*. *49* 329-339,

[14] Liu,Y., Cheng, B., Barbera, G., Troolin, D. R., Deng, X. (2013) Volumetric visualization of the near-and far-field wake in flapping wings. *Bioinspiration and Biomimetics*, *8*, 036010,

[15] Cheng, B., Roll, J., Liu, Y., Troolin, D. R., Deng, X. (2014) Three-dimensional vortex wake structure of flapping wings in hovering flight, *Joural of Royal Society Interface*, *11*, 20130984

[16] Henningsson, P., Michaelis, D., Nakata, T., Schanz, D., Geisler, R., Schröder, A., Bomphrey, R. (2015) The complex aerodynamic footprint of desert locusts revealed by large-volume tomographic particle image velocimetry. *Joural of Royal Society Interface*, 12, 20150119,

[17] Varfvinge, K., Johansson, L., Hendenström, A. (2021) Hovering flight in hummingbird hawkmoths: kinematics, wake dyanmics and aerodynamic power, *Journal of Experimental Biology*, *224*, 1-16,

[18] Liu, Y., Roll, J., Van Kooten, S., Deng, X. (2018) Schlieren photography on freely flying hawkmoth. *Biology Letters, 14,* 20180198,

[19] Liu, Y., Lozano, A., Hedrick, T., Li. C., (2021) Comparison of Experimental and Numerical Studies on the Flow Structures of Hovering Hawkmoths. *Journal of Fluids and Structures*, *107*, 103405,

[20] Liu, T., Shen, L. (2008) Fluid flow and optical flow, *Journal of Fluid Mechanics*, *614*, 253-291,

[21] Liu, T. (2017) OpenOpticalFlow: An Open Source Program for Extraction of Velocity Fields from Flow Visualization Images. *Journal of Open Research Software*. *5*: 29

[22] Usherwood, J. R., Cheney, J. A., Song, J., Windsor, S. P., Stevenson, J. P. J., Dieksheide, U., Nila, A., Bomphrey, R. J. (2020) High aerodynamics lift from the tail reduces drag in gliding raptors. *Experiments in Fluids*, 57:70,

[23] Schanz, D., Gesemann, S., Schröder, A.(2016) Shake-The-Box: Lagrangian particle tracking at high particle image densities. *Experiments in Fluids*, 57:70,

[24] Veldhuis, C., Biesheuvel, A., Wijingaarden, L., Lohse, D.(2005) Motion and wake structure of spherical particels. *Nonlinearity*, *18*, C1-C8,

[25] Batchelor, G. K. (2000) An introduction to fluid dynamics, Cambridge University Press.

[26] Agromayor, R., Rua, J., Kristoffersen, R. (2017) *Simulaiton of starting and stopping vortices of an airfoil, Proceeding of the 58th SIMS*, Sep 25th -27th, Reykjavik, Iceland.